International Journal of Heat and Mass Transfer 52 (2009) 1690–1700

Contents lists available at ScienceDirect

International Journal of Heat and Mass Transfer

journal homepage: www.elsevier.com/locate/ijhmt

# Three-dimensional simulation of turbulent forced convection in a duct with backward-facing step

H. Lan, B.F. Armaly *, J.A. Drallmeier

*Department of Mechanical and Aerospace Engineering Missouri University of Science and Technology, 400 West 13th Street, Rolla, MO 65409, USA*

ARTICLE INFO

*Article history:*
Received 11 April 2008
Received in revised form 30 September 2008
Available online 10 December 2008

ABSTRACT

Results from three-dimensional (3-D) simulations of turbulent forced convection adjacent to backward-facing step in a rectangular duct using a $k-\epsilon-\zeta-f$ turbulence model are reported. This turbulence model is numerically robust near the wall, and it has been shown to predict turbulent heat transfer in separated and wall-bounded flows better than commonly used two-equation turbulence models. FLUENT-CFD code is used as the platform for these simulations and User Defined Functions (UDF) are developed for incorporating this turbulence model into the code. The UDF implementation is validated by simulating several 2-D separated flow/heat transfer benchmark problems. The resulting excellent agreements between the simulated results and benchmark data for these 2-D problems justify the use of this resource for simulating 3-D convection problems. Three-dimensional backward-facing step geometry with an expansion ratio of 1.48 and with a step height of 4.8 mm is used in this study. Three aspect ratios of 3, 8 and infinity (2-D simulation) are considered for studying its effect on the flow and heat transfer, and similarly the effect of the Reynolds number was examined by varying its magnitude in the range of 20,000–50,000. Simulated results are presented for the general 3-D flow features, the reattachment lines, temperature and Nusselt number distributions that develop in this geometry.



## 1. Introduction

Flow separation and reattachment that are caused by a sudden change in geometry occur in many heat-exchanging devices, and 3-D effects are significant in these applications. The heat transfer rate varies greatly in the recirculation flow region due to the 3-D flow behaviors, and accurate heat transfer prediction could improve and optimize the design of such devices. The separated flow over a backward-facing step has received a great deal of attention, and lots of 2-D laminar [1–2], 2-D turbulent [3–6] and 3-D laminar [7–14] flow and heat transfer studies have been published for this geometry. Relatively few numerical simulations for 3-D turbulent flow and convective heat transfer [15–17] have been published, and the need for a more reliable turbulence model to accurately predict the turbulent heat transfer has been cited in the above references. To the authors' knowledge, simulations of turbulent forced convection in 3-D separated flow using recent and improved turbulence models have not appeared in the literature and that motivated this study.

The $k-\varepsilon$ turbulence model has been used extensively in simulating turbulent flow, but it has been shown to fail in accurately predicting heat transfer in separated flows. Nie and Armaly [16] have reported that simulations using the Low-Re $k-\varepsilon$ turbulence model resulted in reasonable agreement with flow measurements but poor agreement with heat transfer measurements. It was also reported in [4] that commonly used two-equation turbulence models generate inaccurate predictions for normal Reynolds stress due to the use of isotropic eddy viscosity. Recent turbulence models, which account for turbulence anisotropy, such as $\bar{v}^2-f$ model and its modified versions [18–19], have improved significantly the heat transfer prediction in separated flows. As a subset of that model, the $k-\varepsilon-\zeta-f$ turbulence model [20] offers the benefit of being numerically robust and has been shown to simulate well the heat transfer in a variety of 2-D turbulent separated flow problems; hence the turbulence model is utilized in this 3-D study.

## 2. Description of turbulence model

The $k-\varepsilon-\zeta-f$ turbulence model was developed from the original $\bar{v}^2-f$ model [18] by replacing the $\bar{v}^2$-equation with a $\zeta$-equation where $\zeta=\bar{v}^2/k$, the ratio of wall-normal Reynolds stress to turbulent kinetic energy. It has been shown that the new equation for $\zeta$ is more robust numerically than the $\bar{v}^2$ equation and that results in improved numerical stability [20]. A quasi-linear pressure-strain model is also applied in the $f$-equation with additional improvements for simulating non-equilibrium wall-bounded flows [20].

The governing equations for turbulent forced convection together with the $k-\varepsilon-\zeta-f$ turbulence model [20] and the corresponding boundary conditions are listed below:

* Corresponding author. Tel.: +1 573 341 4601; fax: +1 573 341 4609.
*E-mail address:* armaly@mst.edu (B.F. Armaly).

0017-9310/$ - see front matter © 2008 Elsevier Ltd. All rights reserved.
doi:10.1016/j.ijheatmasstransfer.2008.09.022

**Nomenclature**

| | |
|---|---|
| $C_p$ | thermal specific heat (J kg$^{-1}$ K$^{-1}$) |
| $AR$ | aspect ratio, $AR = 2L/h$ |
| $D$ | nozzle diameter (m) |
| $ER$ | expansion ratio, $ER = H/h$ |
| $f$ | elliptic relaxation function |
| $G_k$ | turbulent kinetic energy production (times density) (kg m$^{-1}$ s$^{-3}$) |
| $h$ | duct height upstream of the step (m) |
| $H$ | duct height downstream of the step (m) |
| $k$ | turbulent kinetic energy (m$^2$ s$^{-2}$) |
| $k^+$ | non-dimensional turbulent kinetic energy, $k^+ = k/u_\tau^2$ |
| $L$ | half of the duct width (m) |
| $L_t$ | turbulent length scale (m) |
| $Nu$ | local Nusselt number, $Nu = q_{wD}/\lambda(\bar{T}_w - \bar{T}_{in})$ |
| $Nu_b$ | bulk Nusselt number, $Nu_b = q_{wD}/\lambda(\bar{T}_{w,avg} - \bar{T}_b)$ |
| $Pr_t$ | turbulent Prandtl number |
| $q_w$ | heat flux (W m$^{-2}$) |
| $r$ | radius from the jet impingement center point (m) $Re_\tau$ Reynolds number, $u_\tau\delta/\nu$ |
| $Re_h$ | Reynolds number, $Re_h = U_b h/\nu$ |
| $S$ | step height (m) |
| $\bar{S}$ | strain rate magnitude (s$^{-1}$) |
| $S_{ij}$ | strain rate tensor (s$^{-1}$) |
| $\bar{St}$ | stanton number, $St = q_w/[\rho U_{ref} C_p(\bar{T}_w - \bar{T}_{in})]$ |
| $T$ | turbulent time scale (s) |
| $\bar{T}$ | local temperature (K) |
| $\bar{T}_b$ | bulk flow temperature $\bar{T}_b = \int\int U\bar{T}dydz/\int\int Udydz$ (K) |
| $\bar{T}_{w,avg.}$ | averaged bottom wall temperature, $\bar{T}_{w,avg.} = \int_0^L \bar{T}_w dz/L$ (K) |
| $U_b$ | bulk average velocity (m s$^{-1}$) |
| $U_i$ | velocity component (m s$^{-1}$) ($U_i$ is $U$, $V$, $W$ in $X$-, $Y$-, $Z$-direction, respectively) |
| $U_{ref}$ | reference velocity (m s$^{-1}$) |
| $u_\tau$ | friction velocity, $u_\tau = \sqrt{\tau_w/\rho}$ (m s$^{-1}$) |
| $\bar{v}^2$ | wall-normal Reynolds stress component (m$^2$ s$^{-2}$) |
| $x_i$ | coordinate vector component (m) |
| $X_r$ | reattachment point (m) |
| $X_s$ | separation point (m) |
| $y$ | distance from the wall (m) |
| $y^+$ | non-dimensional wall coordinate, $y^+ = yu_\tau/\nu$ |

*Greek symbols*

| | |
|---|---|
| $\delta$ | half channel height (m) |
| $\varepsilon$ | turbulent dissipation rate (m$^2$ s$^{-3}$) |
| $\lambda$ | thermal conductivity (W m$^{-1}$ K$^{-1}$) |
| $\mu_t$ | turbulent viscosity (kg m$^{-1}$ s$^{-1}$) |
| $\nu$ | kinematics viscosity (m$^2$ s$^{-1}$) |
| $\rho$ | density (kg m$^{-3}$) |
| $\zeta$ | $\bar{v}^2/k$ |

*Subscripts*

| | |
|---|---|
| in | inlet of the computational domain |
| w | wall |
| avg. | averaged value |

$$\frac{\partial \rho U_i}{\partial x_i} = 0 \tag{1}$$

$$\frac{\partial}{\partial x_j}(\rho U_i U_j) = -\frac{\partial p}{\partial x_i} + \frac{\partial}{\partial x_j}\left[(\mu + \mu_t)\left(\frac{\partial U_i}{\partial x_j} + \frac{\partial U_j}{\partial x_i}\right)\right] \tag{2}$$

$$\frac{\partial}{\partial x_j}(\rho U_j \bar{T}) = \frac{\partial}{\partial x_j}\left(\left(\frac{\mu}{Pr} + \frac{\mu_t}{Pr}\right)\frac{\partial \bar{T}}{\partial x_j}\right) \tag{3}$$

$$\frac{\partial}{\partial x_j}(\rho U_j k) = \frac{\partial}{\partial x_j}\left[(\mu + \mu_t)\frac{\partial k}{\partial x_j}\right] + G_k - \rho\epsilon \tag{4}$$

$$\frac{\partial}{\partial x_j}(\rho U_j \epsilon) = \frac{\partial}{\partial x_j}\left[\left(\mu + \frac{\mu_t}{1.3}\right)\frac{\partial \epsilon}{\partial x_j}\right] + \frac{C_{\epsilon 1} G_K + 1.9\rho\epsilon}{T} \tag{5}$$

$$\frac{\partial}{\partial x_j}(\rho U_j \zeta) = \frac{\partial}{\partial x_j}\left[\left(\mu + \frac{\mu_t}{1.2}\right)\frac{\partial \zeta}{\partial x_j}\right] + \rho f - \frac{\zeta G_k}{k} \tag{6}$$

$$L_t^2 \nabla^2 f - f - \frac{1}{T}\left(0.4 + \frac{0.65 G_k}{\rho\epsilon}\right)\left(\zeta - \frac{2}{3}\right) = 0 \tag{7}$$

where

$$\mu_t = 0.22\zeta k T \tag{8}$$

$$C_{\epsilon 1} = 1.4(1.0 + 0.012/\zeta) \tag{9}$$

$$T = \max\left[\min\left(\frac{k}{\epsilon}, \frac{0.6}{0.22\sqrt{3}\zeta\bar{S}}, 85\frac{\nu^3}{\epsilon}\right)^{0.25}\right] \tag{10}$$

$$L_t = 0.36\max\left[\min\frac{k^{1.5}}{\epsilon}, \frac{k^{0.5}}{0.22\sqrt{3}\zeta\bar{S}}, 85\left(\frac{\nu^3}{\epsilon}\right)^{0.25}\right] \tag{11}$$

$$\bar{S} = \sqrt{2_{ij}S_{ij}} \tag{12}$$

$$S_{ij} = \frac{\partial U_i}{\partial x_j} + \frac{\partial U_j}{\partial x_i} \tag{13}$$

$$G_k = \mu_t\left(\frac{\partial U_i}{\partial x_j} + \frac{\partial U_j}{\partial x_i}\right)\frac{\partial U_i}{\partial x_j} \tag{14}$$

where $T$ and $L_t$ are turbulent time scale and turbulent length scale respectively. In this model, a constant turbulent Prandtl number $Pr_t = 0.9$ is used when solving the energy equation. The wall boundary condition is fairly simple. All the variables vanish to zero when a wall is approached except for $\varepsilon$ and $f$:

$$\epsilon_w = \lim_{y\to 0}\frac{2\nu k}{y^2}, \quad f_w = \lim_{y\to 0}\frac{-2\nu\zeta}{y^2} \tag{15}$$

User Defined Functions (UDFs) were developed and added to the FLUENT-CFD code for solving the four turbulence model equations (Eqs. (4)–(7)) together with other governing equations for the flow and thermal fields. Although the source term in Eq. (4) is theoretically exact, some treatment is needed in the numerical realization stage of the simulation. The turbulent dissipation rate, $\varepsilon$ which appears as a source term in that equation, is numerically realized by $\epsilon_{i,j}^n = k_{i,j}^n/T_{i,j}^{n-1}$ instead of using its value from the previous iteration as $\epsilon_{i,j}^n = \epsilon_{i,j}^{n-1}$. The use of either one of these expressions produces similar flow results; however, using the former numerical expression in the simulation produces much better heat transfer results that agree well with reported measurements. This treatment is similar to the one that has been utilized in the process of developing Eq. (5) from the $\varepsilon$-equation that appears in the standard $k-\varepsilon$ turbulence model.

The governing equations are solved by a segregated solver, and the SIMPLEC algorithm is used to deal with the coupling between the flow field and pressure field. The PRESTO! scheme is used for pressure correction equation, and the QUICK scheme is used for all other equations (see the FLUENT manual for details [21]).

## 3. Model validation

The developed UDF code for this turbulence model is tested and validated by comparing simulated results with available 2-D benchmark data. The results for four of these benchmark cases are presented below. Properties for air that are used in the numerical validation are evaluated at a static temperature of 293 K and are listed as: density $\rho = 1.225$ kg/m$^3$; molecular

viscosity $\mu = 1.81e-5$ kg/m/s; specific heat capacity $C_p = 1005$ J/kg/k; thermal conductivity $\lambda = 0.0242$ W/m/k. Grid-independent solutions were obtained for each of the simulated benchmark cases that are presented in this study.

The first benchmark case is a 2-D channel flow at a Reynolds number of $Re_\tau = 590$ [22]. In this study, a duct height of 1.5 cm and bulk air velocity of 22 m/s are used for generating the above Reynolds number. The non-dimensional velocity distribution and turbulence scalars ($k$ and $\zeta$) distributions versus the non-dimensional wall coordinate in fully developed flow regime are presented in Fig. 1. It is shown that the simulated results for both time-averaged mean velocity and turbulent quantities generated from using the $k-\varepsilon-\zeta-f$ turbulence model compare very well with the corresponding DNS data. The second benchmark case is turbulent forced convection adjacent to a 2-D backward-facing step in a rectangular duct (top wall is parallel to bottom wall) with large aspect ratio. Vogel and Eaton [5,23] measured the flow and heat transfer in this geometry (step height of $S = 3.79$ cm, upstream duct height of $h = 15.16$ cm and expansion ratio of $ER = 1.25$) for a Reynolds number of 28,000 (based on the step height and an inlet free stream velocity of 11 m/s). The inlet air flow is isothermal with a developing velocity boundary layer thickness of 1.1 $S$. The air $U_{ref}$ flow enters the upstream section of the duct at a location of three times step height upstream from the backward-facing step location. The simulated reattachment length for this case is $X_r = 7.1S$ as compared to the measured value of $X_r = 6.7\ S$ (a difference of less than 6%). Heat transfer measurements in the same geometry were reported in Ref. [23] where a uniform heat flux of 270 W/m$^2$ was supplied on the stepped wall (downstream from the sudden expansion) while keeping the other walls insulated. Simulated mean velocity and Stanton number distributions compare well with measured values as shown in Fig. 2. The velocities in Fig. 2 are normalized by a reference velocity of = 11 m/s. The results from using the AKN Low-Reynolds number turbulence model [6] are also presented in this figure to illustrate the error in the Stanton number (more than 30%) resulting from using that turbulence model.

The third benchmark case is the flow and heat transfer resulting from a normally-impinging round jet on a heated flat plate [24], for which measured data is available for Reynolds number of 23,000 (based on upstream bulk velocity and nozzle diameter of D = 2.6 cm) in the ERCOFTAC database. Fully developed flow is discharged from the nozzle at a distance (above the heated plate) of two times the nozzle diameter. The flat plate is heated by a uniform heat flux of $q_w = 300$ W/m$^2$. Simulated results compare well with benchmark data as shown in Fig. 3 for the velocity distribution and the Nusselt number distribution. Simulated results using the AKN Low-Re $k-\varepsilon$ turbulence model [6] are also presented in these figures for comparison, i.e. poor heat transfer prediction in the stagnation flow region although acceptable near-wall velocity distribution is obtained at most of the streamwise locations.

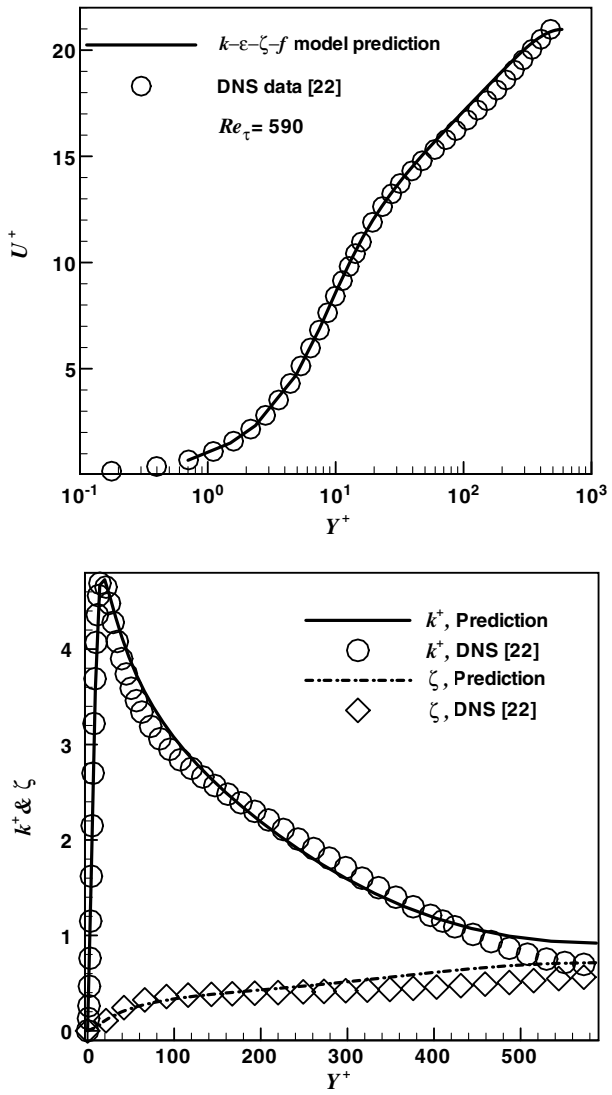


**Fig. 1.** Velocity and turbulence scalars distribution in channel flow at $Re_\tau = 590$.

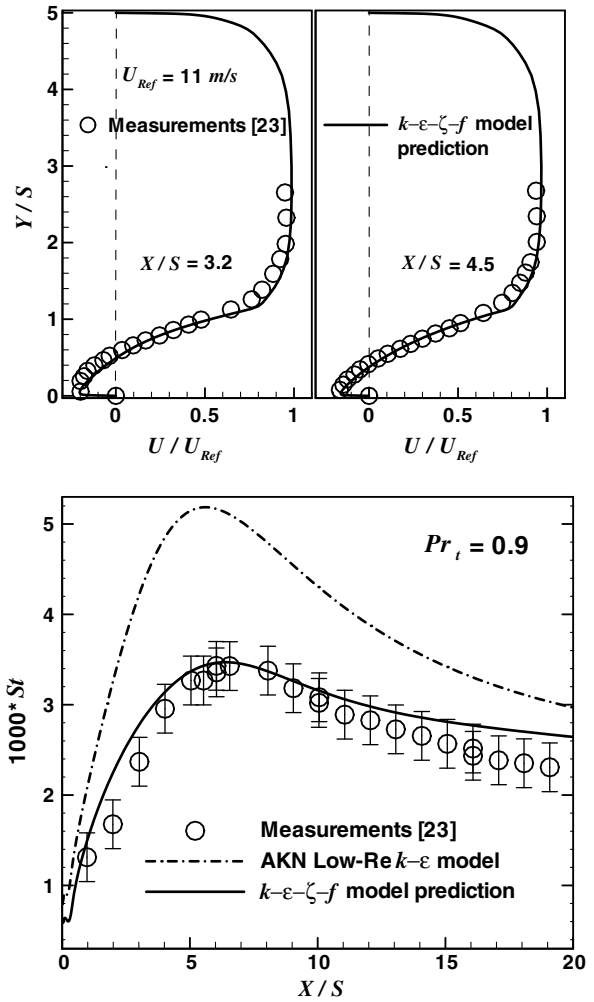


**Fig. 2.** Velocity and Stanton number distributions in backward-facing step flow.

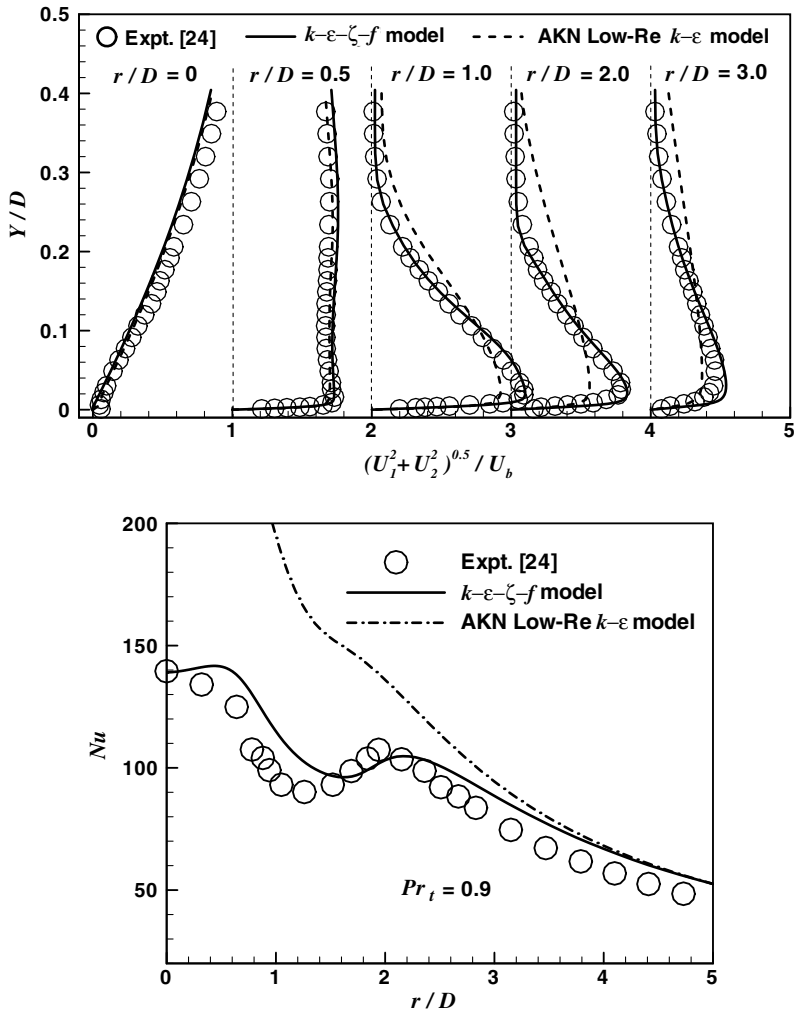


**Fig. 3.** Velocity and Nusselt number distributions for normally-impinging jet flow.

The fourth benchmark case is another 2-D backward-facing step flow where the reattachment length is measured as a function of the Reynolds number by Makiola and Ruck [25]. The backward-facing step geometry had an expansion ratio of 1.48; a step height of 12 mm and the Reynolds number was varied from 15,000 to 64,000 (based on upstream duct height and maximum upstream velocity). Simulated results are compared with measured values in Fig. 4 showing a difference of less than 5% for the cases with Reynolds number greater than 20,000. Considering the experimental uncertainties, the agreement between simulations and measurements is good.

The good agreement between simulated results and benchmark data for the above four cases validated the implementation of the developed UDF code for incorporating the $k-\varepsilon-\zeta-f$ turbulence model in the FLUENT-CFD platform and justifies its use in simulating other 2-D and 3-D convection problems in separated flow. The required CPU time for simulation using this model is about 1.25 times of that required when using the standard $k-\varepsilon$ turbulence model. Considering the improved flow and heat transfer predictions, the additional computational cost is moderate and cost effective.

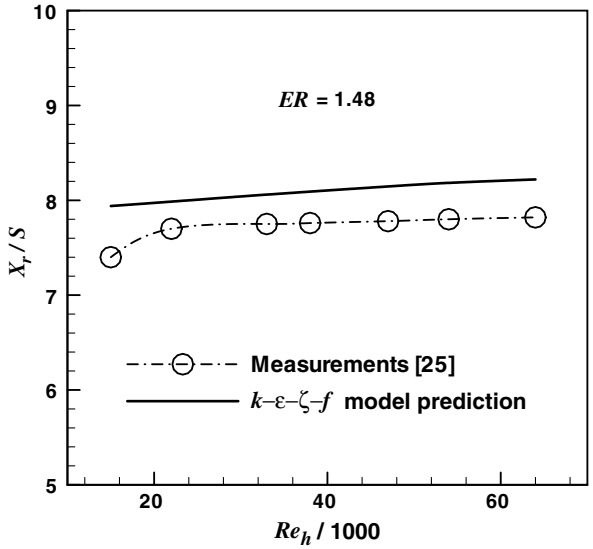


**Fig. 4.** Reattachment length for 2-D backward-facing step flow.

## 4. Problem statements and its simulation

The 3-D backward-facing geometry that is used in this study has the same expansion ratio as the one examined by Makiola and Ruck [25]. Several aspect ratios and Reynolds numbers are considered in order to examine their effects on both flow and heat

transfer. The geometry and the computational domain are shown schematically in Fig. 5. It consists of a plane horizontal duct with a backward-facing step. The upstream duct height is $h = 10$ mm and the downstream duct height is $H = 14.8$ mm, resulting in an expansion ratio of $ER = H/h = 1.48$ and the step height of $S = 4.8$ mm. The lengths of the computational domain are 14.4 mm upstream and 360 mm downstream of the step respectively, i.e. $-3 = X/S = 75$. Simulations using a longer downstream length of 450 mm results in less than 1% change in the reattachment length. The origin of the coordinate system is located at the bottom corner of the step where the sidewall, the backward-facing step, and the downstream stepped wall (bottom wall) intersect, as shown in Fig. 5. Fully developed turbulent flow with a uniform temperature of $T_{in} = 293$ K is introduced in the upstream duct at the inlet plane at $X/S = -3$, and a pressure outlet boundary condition is imposed at the exit plane of the computational domain, i.e. at $X/S = 75$. A uniform and constant heat flux of $q_w = 800$ W/m$^2$ is supplied on the downstream stepped wall while all the other walls are treated as adiabatic, and no-slip boundary condition is used for all the bounding walls. Due to flow and thermal symmetry in the spanwise direction, the width of the computational domain is chosen as $L$, which is half of the actual width of the duct; and symmetry boundary condition is applied at the center plane, i.e. at $Z = L$. The physical properties are treated as constants and the values are the same as the ones listed in the "model validation" section. The inlet profiles that are used at $X/S = -3$ plane are obtained from a separate computation for fully developed flow in a duct with height $h = 10$ mm with a length of 1000 mm ($100h$). The inlet streamwise velocity component to that duct is taken to be uniform and calculated for a specific Reynolds number, and the other two velocity components, $V$ and $W$, are taken as zero. The inlet turbulent kinetic energy ($k$) and the dissipation rate ($\varepsilon$) to that duct are automatically calculated in the FLUENT-CFD code from the supplied turbulence intensity ($TI = 10\%$) and the hydraulic diameter of the duct ($D_h = 2\,AR\,h/(1 + AR)$). Simulations are performed for three Reynolds numbers ($Re_h = U_b h/\nu$, where $U_b$ is the inlet bulk velocity and $h$ is upstream duct height) of 22,000, 33,000 and 47,000 and for three aspect ratios of 3, 8 and infinity (2-D simulation).

Non-uniformly structured mesh and hexahedron volume elements are used in the simulations. The grid points cluster in all near-wall regions ($y^+$ values for all the first near-wall grid points are always less than unity), in the reattachment zone and in the separated shear layer. A grid of $100 \times 90 \times 60$ ($X \times Y \times Z$) downstream of the step was used for simulating the case of $AR = 3$, and 30 more grid points in Z-coordinate ($X \times Y \times Z = 100 \times 90 \times 90$) were used for the case of $AR = 8$. Grid independence studies were made with different grid densities and distributions by using the reattachment line, velocity and turbulent scalars ($U$, $k$, $\zeta$) distributions as the criteria. For example, with aspect ratio of 3, using three other meshes ($140 \times 90 \times 60$ [mesh 1], $100 \times 120 \times 60$ [mesh 2], $100 \times 90 \times 80$ [mesh 3]) resulted in less than 2% difference in the predicted location of the reattachment line. The predicted distributions from using the three different meshes are almost the same as shown in the Fig. 6 for the variables like $U$, $k$ and $\zeta$. The computation is considered as converged when the residuals for all the variables are smaller than $10^{-6}$.

## 5. Results and discussions

The general flow features in this geometry are presented in Fig. 7 for the case of $AR = 3$ and Reynolds number of $Re_h = 22{,}000$. Similar flow features develop in this geometry with other aspect

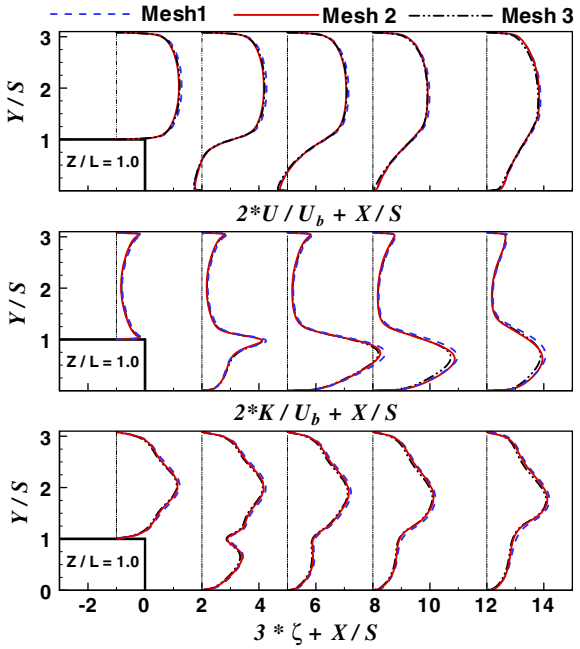


**Fig. 6.** Grid-independence study for this simulation.

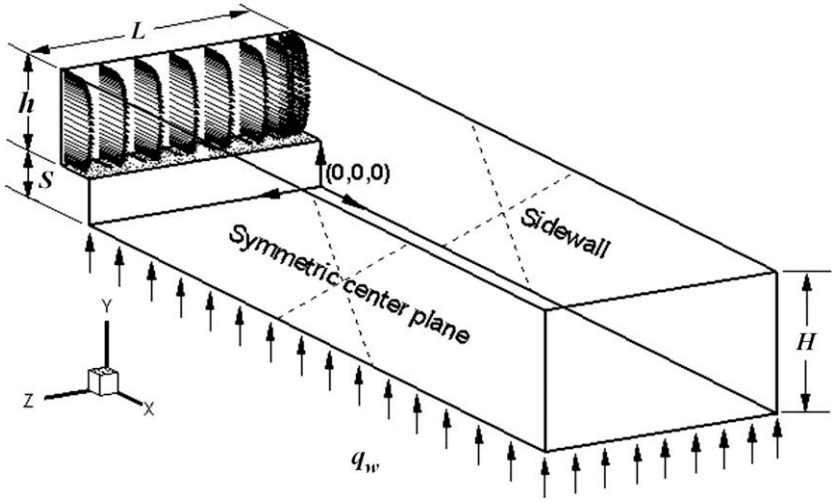


**Fig. 5.** Schematic of the 3-D backward-facing step geometry.

ratio and for that reason the flow features are reported for only one case. Several streamlines that originate from a region close to the side wall at the inlet plane are presented to illustrate some of the flow features that develop in this geometry. The vortex flow that develops due to the sudden expansion in this geometry can be clearly seen in this figure. The swirling spanwise flow that develops adjacent to the step moves toward the center of the duct and forms the primary recirculation flow region. The "jet-like" flow that develops adjacent to the side wall impinges on the bottom wall and acts as a source point that distributes its flow in all directions adjacent to the bottom wall. Limiting streamlines near the side wall and the bottom wall of the duct are presented in this figure to illustrate this behavior. A near-wall plane with a normal distance away from the wall as 0.01 $S$ is used to display the limiting streamlines that are shown in this figure. Three reversed flow regions are shown in this figure, and two of them are adjacent to the bottom wall (the bigger one is designated as primary recirculation flow region and the smaller one near the step is designated as secondary recirculation flow region) and the third one is adjacent to the top wall of the duct. The boundaries of the recirculation flow regions are presented by dashed lines in this figure and that designate the locations where the near-wall streamwise velocity component (at $Y/S = 0.01$) is zero. The "source" point that appears on the bottom wall and near the side wall (at approximately $Z/L = 0.1$) is the impingement location of the "jet-like" flow. The dashed line on the bottom wall that separates the reversed and the streamwise fractions of the flow is the reattachment line, and the impingement point is located on that line.

The effect of the Reynolds number and the aspect ratio on the reattachment line and the boundaries of the recirculation flow regions (as determined by the location where the streamwise velocity component is equal to zero on a plane $Y = 0.01S$) is shown in Fig. 8. The results show that these lines are not affected significantly by the Reynolds number in this turbulent flow regime. For the aspect ratio ($AR = 3$) the reattachment length is almost constant for 30% of the duct's width and starts to increase rapidly as it approaches the side wall (when $Z/L < 0.3$), reaching a maximum at the side wall. The effect of the aspect ratio on the reattachment line is significant only in the region near the sidewall. The 2-D results are also presented in this figure for comparison and it can be seen that even for the case of $AR = 8$ the side wall effect on the reattachment line continues to be significant at the center of the duct ($Z/L = 1$) (half step height difference in the reattachment length as compared with 2-D results).

The following general observations can be made relative to the velocities and the turbulence in the flow downstream of the step. Figures illustrating their behaviors are not included in the manuscript due to space limitations. The mean streamwise velocity component ($U$) outside the recirculation flow region increases as the distance from the side wall increases, but that component inside

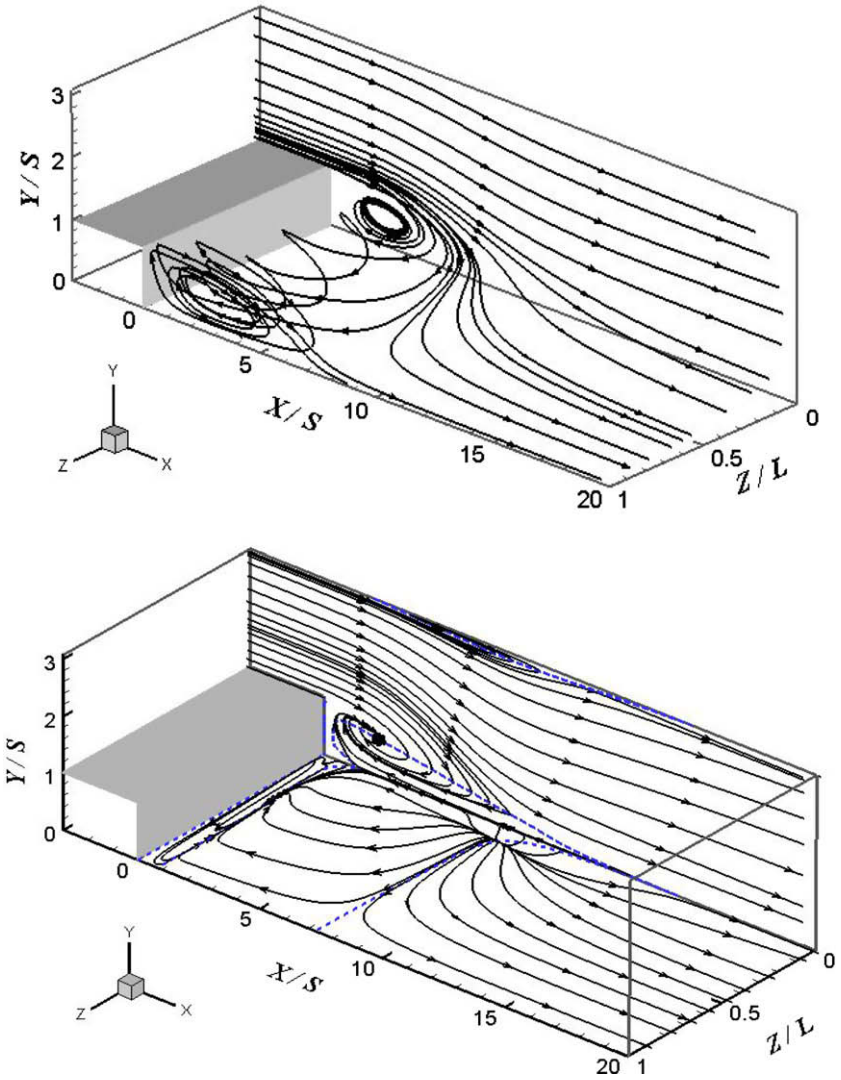


**Fig. 7.** General flow behavior and limiting streamlines for backward-facing step ($AR = 3$).

the recirculation flow region (reverse flow direction) reaches a maximum in magnitude near the side wall due to the "jet-like" flow. As the aspect ratio decreases this velocity component decreases near the side wall but increases at the center of the duct. The mean transverse velocity component ($V$) is negative in most of the flow domain and it develops a negative peak near the region where the "jet-like" flow impinges on the bottom wall of the duct, and the peak magnitude of that velocity component increases when the aspect ratio is decreasing. The mean spanwise velocity component ($W$) is positive in most of the flow domain and continues to be significant in the neighborhood of the reattachment line and in the region downstream of that line. A maximum in that velocity component develops near the side and bottom walls of the duct at a location that is further away from the side wall than the impingement location of the "jet-like" flow. Decreasing the aspect ratio of the duct decreases the magnitude of that velocity component. The turbulent kinetic energy ($k$) develops a peak in the region of the separating shear layer and its magnitude increases as the distance from the side wall increases. Turbulent kinetic energy ($k$) and turbulence anisotropy $\zeta$ increase in the region near the side wall as the aspect ratio increases but the effect of the aspect ratio diminishes at the center of the duct.

The temperature distribution on the heated bottom wall of the duct is presented in a contour format in Fig. 9 for a duct with aspect ratio of 3. The reattachment line and the "jet-like" flow impingement location (the source point illustrated by several limiting streamlines on the near-wall plane at $Y = 0.01S$) are also shown in the same figure for reference. The streamlines are identified by the lines with arrows; while the reattachment line is identified by the thicker line and spans across the width of the duct. Generally, it shows that the increase in Reynolds number results in lower bottom wall temperature, i.e. the convective heat transfer is enhanced by increasing the fluid velocity. The bottom wall temperature develops a minimum in a location inside the primary recirculation flow region, and that coolest spot on that wall is about one step height upstream from the "jet-like" flow impingement location and further away than that point from the side wall. The lower wall temperature corresponds to the location where the convection heat transfer coefficient is higher, so that the location of the coolest spot is associated with the maximum local Nusselt number on that wall. In the figure, the 'jet-like" flow impingement location is identified by a circle symbol; and the location of maximum local Nusselt number is identified by a square box. It should be noted that in the laminar flow regime the location of the maximum local Nusselt number and the "jet-like" flow impingement location on the heated bottom wall are very close to each other [8]; however, in the turbulent flow regime they are farther apart from each other as shown in Fig. 9. The reason for that difference can be attributed to the relatively high spanwise velocity component that develops near the bottom wall as shown in Fig. 10 which illustrates the distribution of the spanwise velocity component on a near-wall plane of $Y = 0.01S$ (contour lines and color). The same limiting streamlines and identical symbols for the two important locations are included in this figure as the ones presented in Fig. 9. The locations of the maximum spanwise velocity component at that plane ($Y = 0.01S$) and the maximum local wall Nusselt number (on the bottom wall) are in the same general region (in both the streamwise and spanwise coordinates), thus implying that this velocity component contributes significantly to the local heat transfer rate.

The magnitude of the near-wall spanwise velocity component influences significantly the magnitude and the location of the lowest wall temperature on the heated wall. The effects of the Reynolds number, the streamwise distance from the step, and the aspect ratio on the spanwise distributions of the local wall Nusselt number (on the bottom wall) and the near-wall spanwise velocity component (at $Y/S = 0.01$ plane) are presented in Figs. 11–13, respectively. It can be clearly seen from Fig. 11 that the locations of maximum local wall Nusselt number and the maximum spanwise velocity component on that plane are almost coincident with each other. The increase in Reynolds number increases both the local wall Nusselt number and the spanwise velocity component on that plane. The results in Fig. 12 show the spanwise distributions of these two variables at different streamwise locations. The two variables have higher magnitude in the reattachment region of the flow than inside recirculation flow region or in the redeveloping flow region downstream from the step. The results in Fig. 13 show the effects of the aspect ratio on the magnitude of the same two variables. The aspect ratio has significant influence on the magnitude of the spanwise velocity component at the near-wall plane but has only small influence on local wall Nusselt number. For an aspect ratio of 3, the two variables reach maximum value at around $Z/L = 0.3$, but for an aspect ratio of 8 the maximum value develops at $Z/L = 0.1$ (note that $L$ is larger for the larger aspect ratio case). It implies that the maximum local wall Nusselt number and maxi-

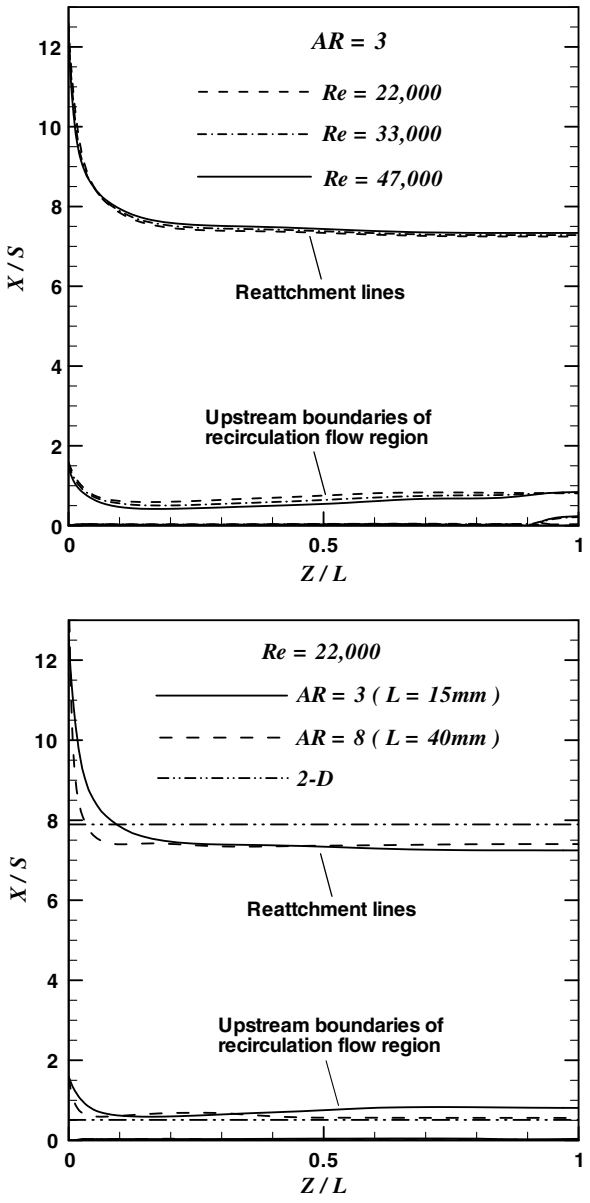


**Fig. 8.** Effects of the Reynolds number and the aspect ratio on reattachment line.

mum spanwise velocity component on that plane develop at similar distance from side wall and that feature is almost independent of the aspect ratio.

The streamwise distribution of the bulk air temperature ($\overline{T}_b$) is presented in Fig. 14 and the results show that the flow with higher Reynolds number generates a lower bulk air temperature. Although the Reynolds number has littler effect on reattachment length, it has significant effect on the heat transfer, the bulk air temperature and the bottom wall temperature. The peak that develops in the bulk air temperature develops inside the recircula-

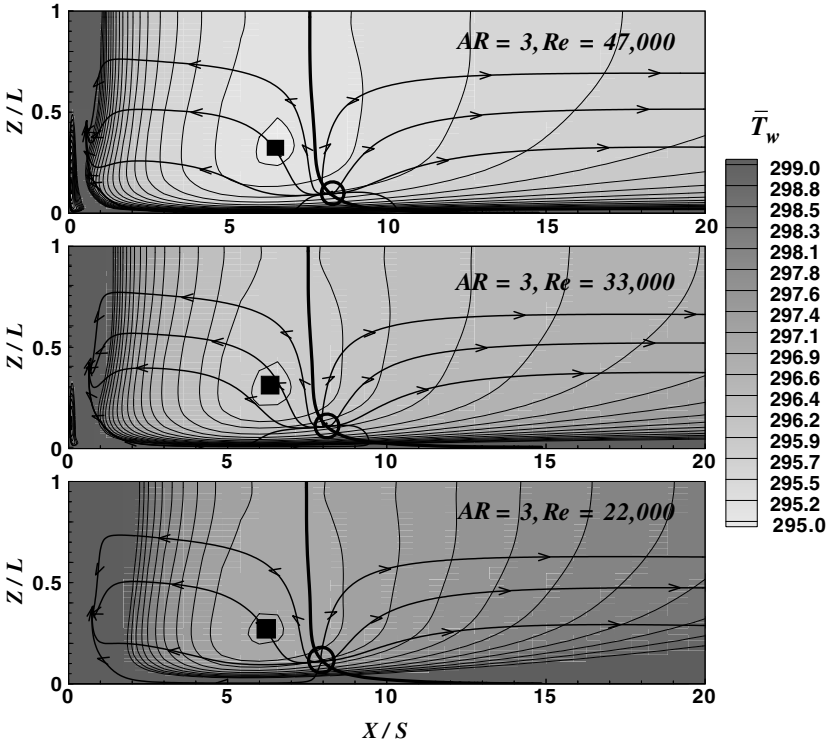


**Fig. 9.** Temperature distribution on the heated bottom wall.

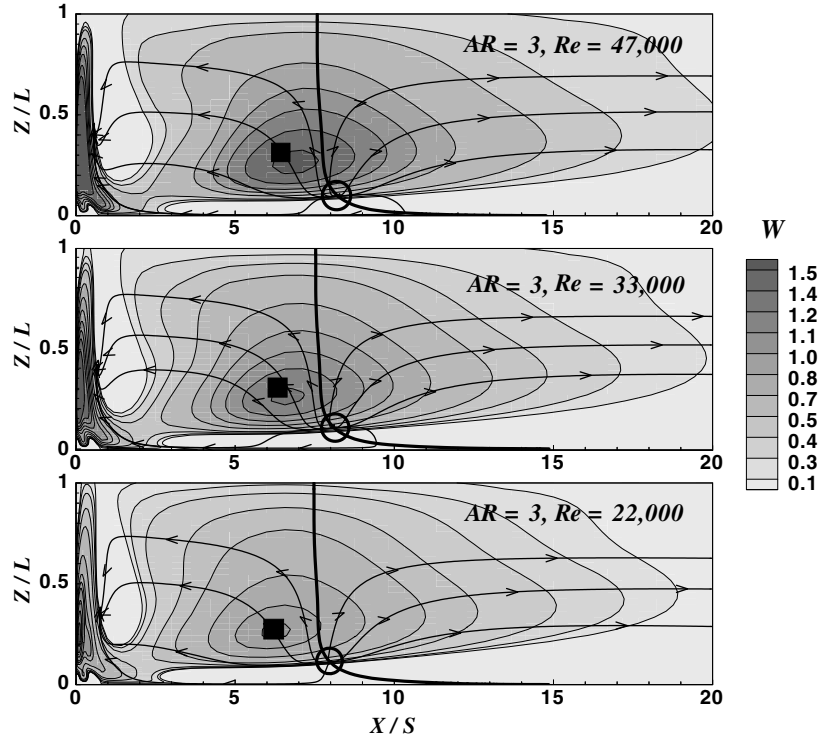


**Fig. 10.** *W*-velocity component on the near-wall plane ($Y = 0.01S$).

tion flow region is followed by a minimum that develops in the flow reattachment region. In the redeveloping flow region (after reattachment), the bulk air temperature increases, and in the fully developed flow region the rate of increase becomes constant. The effects of the Reynolds number and the aspect ratio on the streamwise distribution of the average bottom wall temperature ($\overline{T}_{w,avg.}$) is presented in Fig. 15. The results show that a higher Reynolds number is associated with a lower average wall temperature. The average wall temperature develops a local minimum at two locations; one is inside the secondary recirculation flow region and the other is inside the primary recirculation region where the reverse and spanwise flow increases the heat transfer rate. The average bottom wall temperature develops a global minimum upstream of the reattachment flow region and then it increases at a constant rate in the fully developed flow region. A higher aspect ratio results in a lower average bottom wall temperature. That is due to the fact that the influence of the lower energy region (corresponds to poor heat transfer and high bottom wall temperature) that develops near the side wall becomes insignificant as the aspect ratio of the duct increases.

The effects of the Reynolds number and the aspect ratio on the streamwise distribution of the bulk Nusselt number ($Nu_b$) (based on the bulk air temperature and the average wall temperature) are presented in Fig. 16. Higher Reynolds number or higher aspect ratio is associated with a higher bulk Nusselt number. The results in Fig. 17 illustrate the effects of the aspect ratio on the local Nusselt number (based on the local wall temperature and inlet flow temperature). This Nusselt number is easier to evaluate experimentally by measuring local temperatures (of inlet air flow and bounding walls) and the supplied wall heat flux. The effect of aspect ratio on the local Nusselt number is negligible at the center of the duct but it becomes significant near the

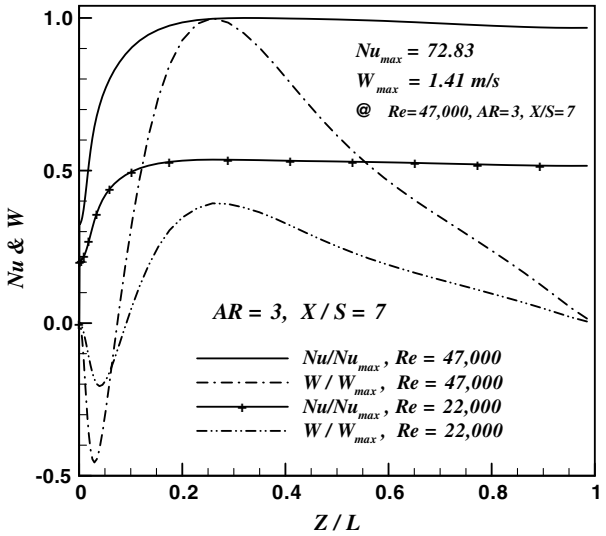


**Fig. 11.** Spanwise distribution of local Nusselt number & the *W*-velocity component at *Y/S = 0.01* (effects of Reynolds number).

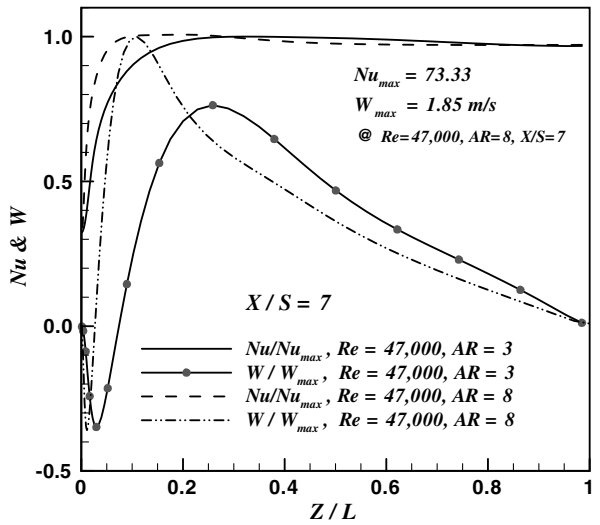


**Fig. 13.** Spanwise distribution of local Nusselt number & the *W*-velocity component at *Y/S = 0.01* (effects of aspect ratio).

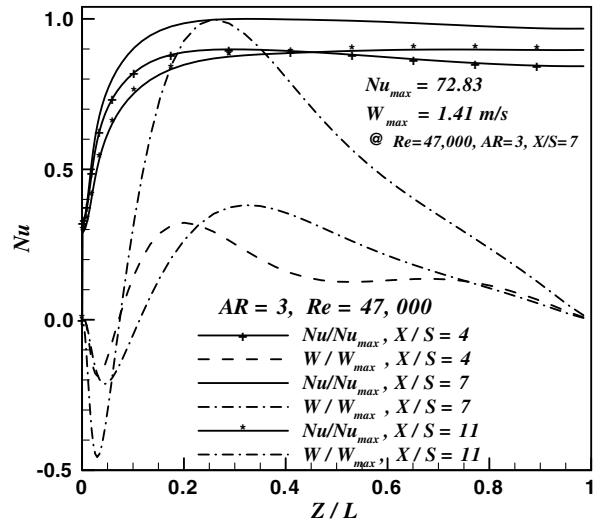


**Fig. 12.** Spanwise distribution of local Nusselt number & the *W*-velocity component at *Y/S = 0.01* (effects of distance from the step).

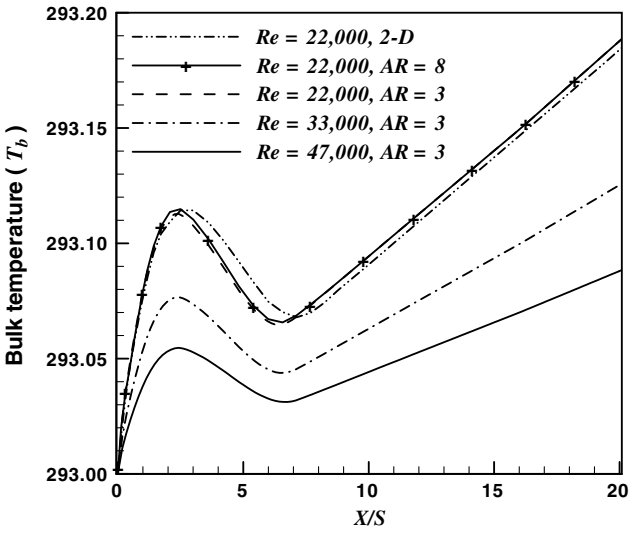


**Fig. 14.** Effects of Reynolds number and aspect ratio on bulk air temperature.

side wall as shown in the figure (for similar Z/L planes). A duct with smaller aspect ratio is associated with a smaller local Nusselt number near the side wall.

## 6. Conclusions

Simulations of three-dimensional turbulent forced convection in a duct with a backward-facing step are reported and the effects of the aspect ratio and the Reynolds number on the flow and the heat transfer characteristics are discussed. The $k-\varepsilon-\zeta-f$ turbulence model that is used in these simulations was shown to be capable of improving significantly the heat transfer predictions in the separated or wall-bounded flows. The effects of the Reynolds number and aspect ratio on the flow reattachment is minimal in the range of parameters that are examined in this study, but they are shown to have significant influence on heat transfer. The reattachment length is constant in central portion of duct width, but starts to increase as it approaches the side walls and reaches its maximum value on the side walls. A "jet-like" flow develops in the separating shear layer near side wall and impinges on the bottom wall of the duct. Significant spanwise flow develops inside the primary recirculation flow region and in the neighborhood of the reattachment line, and that causes the maximum local Nusselt number (lowest wall temperature) to develop in the region where the spanwise velocity component is maximum adjacent to the heated bottom wall (close to the side wall, not at the center of the duct). The increase in Reynolds number results in higher magnitude of near-wall spanwise velocity component and correspondingly results in a higher local wall Nusselt number. The location of the lowest wall temperature on the heated bottom wall is about one step height upstream of "jet-like" flow impingement location and further away from the side wall than that location. The absolute distance of that location from the side wall is not varying significantly with changes in the aspect ratio. That feature differs from the laminar convective flow in the same geometry where the spanwise flow is less significant and the maximum Nusselt number develops closer to the "jet-like" flow impingement region. Increase in the Reynolds number or the aspect ratio results in the higher bulk Nusselt number and lower average wall temperature. The bulk air temperature decreases as the Reynolds number increases, but it is not influenced significantly by changes in the aspect ratio.

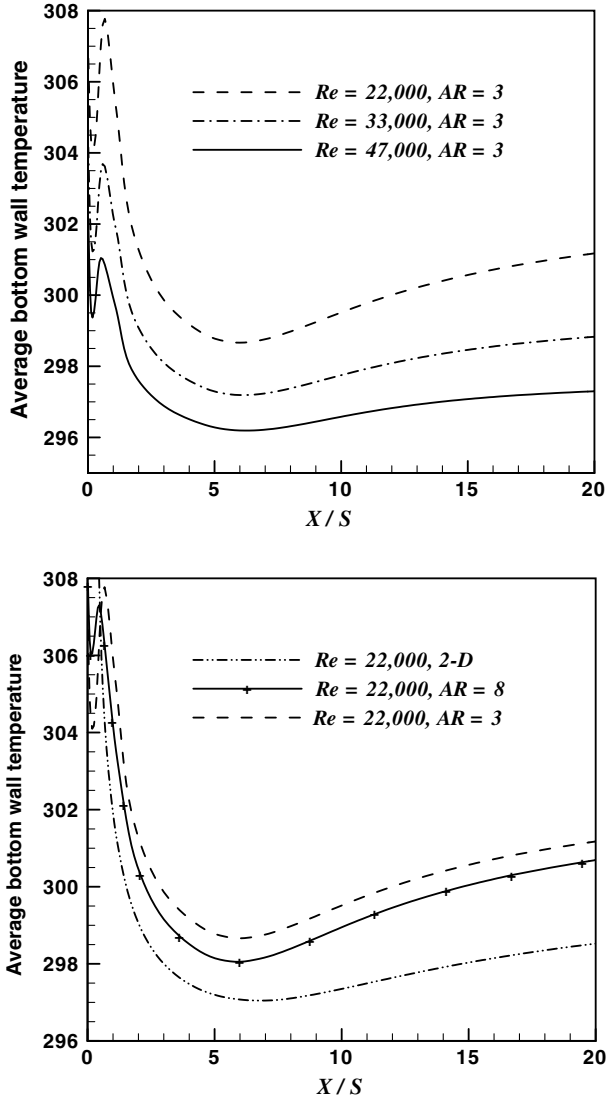


**Fig. 15.** Effects of the Reynolds number and aspect ratio on the average wall temperature.

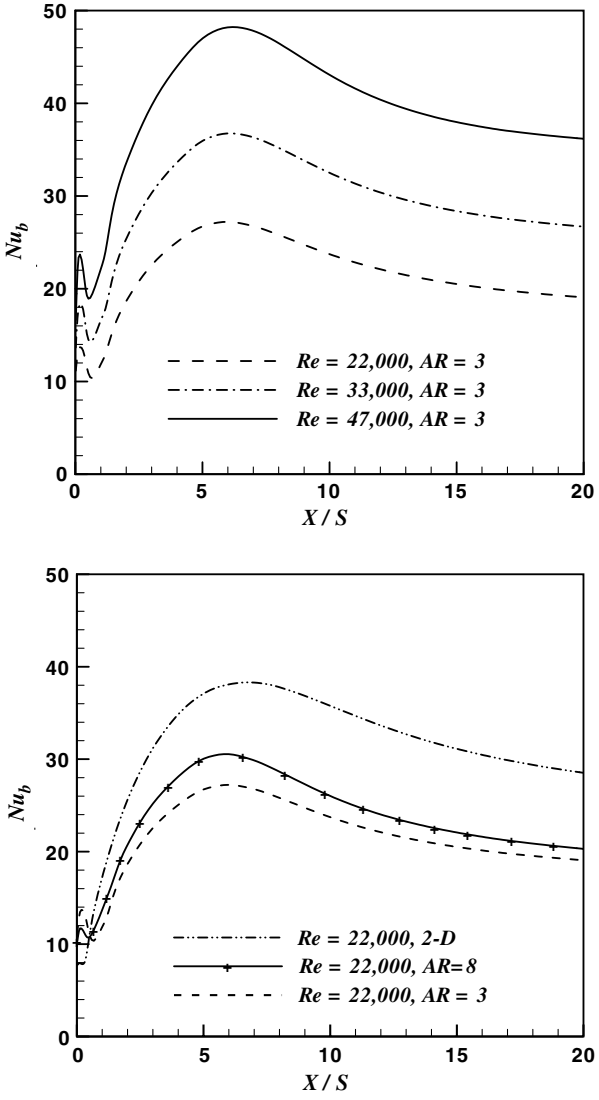


**Fig. 16.** Effects of Reynolds number and aspect ratio on bulk Nusselt number.

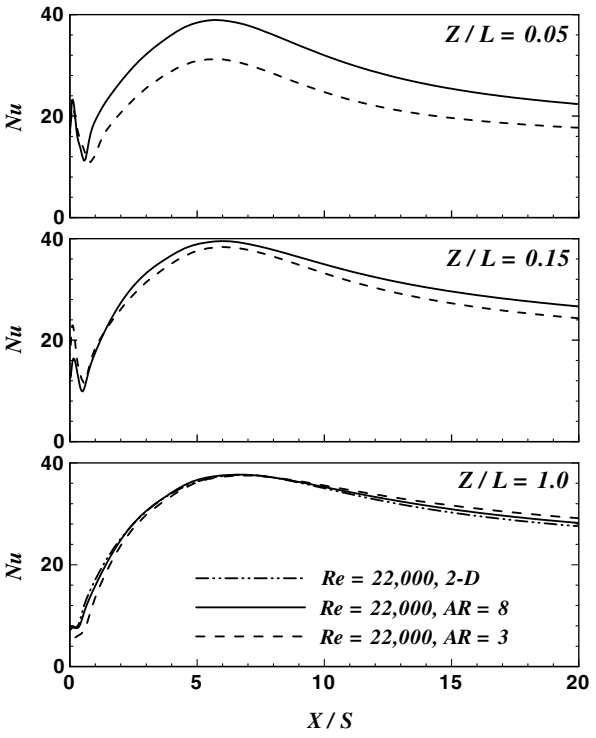


**Fig. 17.** Effects of aspect ratio on local Nusselt number.

## Acknowledgements

This work was supported in part by a DOE-Basic Energy Sciences Grant No. DE-FG02-03ER46067, and by an NSF Grant No. CTS-0352135.

## References

[1] B.F. Armaly, F. Durst, J.C.F. Pereira, B. Schonung, Experimental and theoretical investigation of backward-facing step flow, J. Fluid Mech. 127 (1983) 473–496.
[2] H.I. Abu-Mulaweh, A review of research on laminar convection flow over backward- and forward-facing steps, Int. J. Therm. Sci. 42 (2003) 897–909.
[3] H. Le, P. Moin, J. Kim, Direct numerical simulation of turbulent flow over a backward-facing step, J. Fluid Mech. 330 (1997) 349–374.
[4] S. Thangam, C.G. Speziale, Turbulent separated flow past a backward-facing step a critical evaluation of two-equation turbulence models, AIAA J. 30 (1992) 1314–1320.
[5] J.C. Vogel, J.K. Eaton, Combined heat transfer and fluid dynamic measurements downstream of a backward-facing step, ASME J. Heat Transfer 107 (1985) 922–929.
[6] K. Abe, T. Kondoh, Y. Nagano, A new turbulence model for predicting fluid flow and heat transfer in separating and reattaching flows – I. Flow field calculations, Int. J. Heat Mass Transfer 37 (1994) 139–151.
[7] B.F. Armaly, A. Li, J.H. Nie, Measurements in three-dimensional laminar separated flow, Int. J. Heat Mass Transfer 46 (2003) 3573–3582.
[8] J.H. Nie, B.F. Armaly, Three-dimensional convective flow adjacent to backward-facing step – effects of step height, Int. J. Heat Mass Transfer 45 (2002) 2431–2438.
[9] D.B. Carrington, W. Pepper, Convective heat transfer downstream of 3-D backward-facing step, Numer. Heat Transfer A – Appl. 41 (2002) 555–578.
[10] J.H. Nie, B.F. Armaly, Reattachment of three-dimensional flow adjacent to backward-facing step, J. Heat Transfer 125 (2003) 422–428.
[11] J.G. Barbosa Saldana, N.K. Anand, Forced convection over a three-dimensional horizontal backward-facing step, Int. J. Comput. Meth. Eng. Sci. Mech. 6 (2005) 225–234.
[12] A. Kitoh, K. Sugawara, H. Yoshikawa, T. Ota, Expansion ratio effects on three-dimensional separated flow and heat transfer around backward-facing steps, J. Heat Transfer 129 (2007) 1141–1155.
[13] N. Tylli, L. Kaiktsis, B. Ineichen, Sidewall effects in flow over a backward-facing step: experiments and numerical simulations, Phys. Fluids 14 (2002) 3835–3845.
[14] P.T. Williams, A.J. Baker, Numerical simulations of laminar flow over a 3D backward-facing step, Int. J. Numer. Meth. Fluids 24 (1999) 1159–1183.
[15] K. Kozel, P. Louda, J. Prihoda, Numerical solution of 2D and 3D backward-facing step flows, Proc. Appl. Math. Mech. 5 (2005) 467–468.
[16] J.H. Nie, B.F. Armaly, Three-dimensional turbulent forced convection adjacent to backward-facing step, Turbulent Heat Mass Transfer 4 (2003) 723–730.
[17] S. Yanase, G. Kawahara, H. Kiyama, Three-dimensional vortical structures of a backward-facing step flow at moderate Reynolds numbers, J. Phys. Soc. Jpn. 70 (2001) 3550–3555.
[18] P. Durbin, Separated flow computations with the model, AIAA J. 33 (1995) 659–664.
[19] F. Lien, G. Kalitzin, Computations of transonic flow with the turbulence model, Int. J. Heat Fluid Flow 22 (2001) 53–61.
[20] K. Hanjalic, M. Popovac, M. Hadziabdic, A robust near-wall elliptic-relaxation eddy-viscosity turbulence model for CFD, Int. J. Heat Fluid Flow 25 (2004) 1047–1051.
[21] FLUENT 6.2 User's Guide, FLUENT Inc, 2005.
[22] R. Moser, J. Kim, N. Mansour, Direct numerical simulation of turbulent channel flow up to $Re_\tau = 590$, Phys. Fluids 11 (1999) 943–945.
[23] J.C. Vogel, J.K. Eaton, Heat transfer and fluid mechanics measurements in the turbulent reattaching flow behind a backward-facing step, Report MD-44, Stanford University, 1984.
[24] J. Baughn, S. Shimizu, Heat transfer measurements from a surface with uniform heat flux and an impinging jet, ASME J. Heat Transfer 111 (1989) 1096–1109.
[25] B. Makiola, B. Ruck, Experimental Investigation of a Single-Sided Backward-Facing Step Flow with Inclined Step Geometries, Springer, Berlin, 1990.